JOURNAL OF MATERIALS SCIENCE 32 (1997) 177–184

A photoemission study of the $YBa_2Cu_3O_7$–Au composite

C. HINNEN
Laboratoire de Physico-Chimie des Surfaces, CNRS (URA 425), Université Paris VI, ENSCP, 11 Rue Pierre et Marie Curie, F-75005 Paris Cedex 05, France

C. NGUYEN VAN HUONG
Laboratoire de Physique du Solide, Ecole Supérieure de Physique et de Chimie Industrielles, 10 Rue Vauquelin, F-75231 Paris Cedex 05, France

P.J. GODOWSKI
W. Trzebiatowski Institute for Low Temperature and Structure Research, Polish Academy of Sciences, P.O. Box 937, 50-950 Wrocław, Poland

Characterization of the $YBa_2Cu_3O_7$–Au composite at room temperature has been performed using X-ray photoelectron spectroscopy. Measured spectra on the chemically etched surfaces have been found to be representative of the bulk material. Analysis of the core-level spectra of copper indicated the contribution of the $Cu^{(3+)}$ valence state in the samples. The core-level spectra of gold showed the Au valence state to be between 1 + and 2 +. The incorporated gold atoms had no influence on the level positions of the other constituents of the material.

1. Introduction

In order to understand the high-temperature superconductivity mechanism, the electronic structure of the high-temperature superconductors (HTSC) has been investigated. X-ray photoelectron spectroscopy (XPS), although being a surface-sensitive method, could be adopted for bulk HTSC electronic structure determination [1–3]. Photoelectron spectroscopy, on the basis of the analysis of the core and valence levels, offers the possibility of distinguishing between the HTSC material and other copper compounds. For example, XPS experiments made in the past, showed that the copper oxidation state may reach a value greater than 2 in the high-temperature superconductors.

The $YBa_2Cu_2O_{7-\delta}$ compound is the high-temperature superconducting phase in the Y–Ba–Cu–O system. The orthorhombic structure of this compound of $\delta \leqslant 0.15$ exhibits superconductivity with a transition (critical) temperature, T_c, in the vicinity of 90 K. On the other hand, the tetragonal compound of $\delta \geqslant 0.5$ is a non-superconducting material (e.g. [4]). The lattice structures of the orthorhombic ($a \neq b \neq c$) and tetragonal ($a = b \neq c$) form having three distorted perovskite unit cells stacked along the c-axis, are shown in Fig. 1. The copper atoms are positioned at the corners and the oxygen atoms are on the cube edges. The barium and the yttrium are the ordered metal ions located at the body centred positions of these unit cells in the sequence Ba–Y–Ba along the c-axis. Two inequivalent copper sites, designated Cu1 and Cu2, represent two different structures (the Cu1 chains and the Cu2 planes) in the orthorhombic form, whereas in the case of the tetragonal form, the Cu1 chains are absent. Formal valence could be assigned as: Y^{3+}, Ba^{2+} and O^{2-}. Copper acquires a non-integral valence ranging from 2.00–2.33, i.e. Cu^{2+} and Cu^{3+} mixed valence, depending on the oxygen vacancy concentration, but it is difficult to separate the Cu^{3+}–O^{2-} couple from the Cu^{2+}–O^{2-} one. The content of Cu^{3+}, y, in the $YBa_2Cu_3O_{7-\delta}$ sample is simply calculated using Equation 1.

$$3y + 2(1 - y) = [n_{O} \cdot |-2| - n_{Y} \cdot |+3| - n_{Ba} \cdot |+2|]/n_{Cu} \quad (1)$$

where n_i (i = O, Y, Ba, Cu) denotes the number of i atoms in the chemical formula. For the $YBa_2Cu_3O_7$ specimen, the formal percentage of Cu^{3+} is calculated as 33%.

The purpose of this article is to investigate systematically the $YBa_2Cu_3O_7$ and the $YBa_2Cu_3O_7$–Au composite by XPS and correlate the results with those reported. The spectra of the first sample provide the standard spectra for observation of the electronic structure changes in the second sample, after gold-atom incorporation. During investigation of superconductivity properties, the $(YBa_2Cu_3O_7)_{1-x}$–Au_x composite, with x up to 0.1, showed a little increase in T_c ($\Delta T_c \simeq 1.5$ K) [5–7]. Such behavior needed further electronic structure examination, because the gold atoms incorporated in the $YBa_2Cu_3O_7$ lattice take up

0022–2461

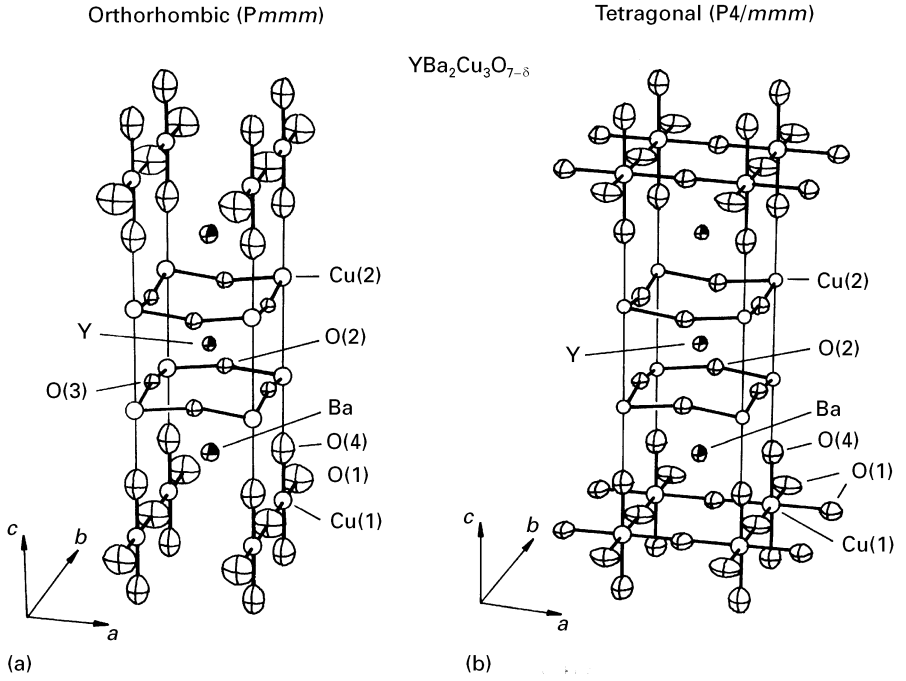

Figure 1 The structure of the $YBa_2Cu_3O_{7-\delta}$ compound: (a) orthorhombic and (b) tetragonal.

the chain Cu1 sites, but it is well known that such a substitution of any atoms always induces degradation of T_c. Gold atoms in the lattice probably will manifest their presence by an influence on the core levels of yttrium, barium, copper and oxygen ions and on the valence band of the sample. With the help of XPS analysis, the oxidation state of gold may be determined, which will provide insight into the nature of the substituted site.

2. Experimental procedure

The $YBa_2Cu_3O_7$ compound was synthesized by solid-state reaction from pure Y_2O_3, $BaCO_3$ and CuO powders mixed in stoichiometric quantities. The mixture was ground, pelletized and reacted in air at 1223 K (950 °C) for 24 h and cooled down to room temperature (RT). The procedure was repeated three times. Finally, the pellet was oxidized in a flowing oxygen atmosphere at 1223 K (950 °C) for 1 h, then at 773 K (500 °C) for 4 h and the furnace was cooled to RT. The YBaCuO–Au composites were prepared from ground $YBa_2Cu_3O_7$ material and gold powder, mixed in the ratio of $(YBaCuO)_{1-x}Au_x$ of $x \leqslant 0.3$. The mixture was sintered in a flowing oxygen atmosphere at 1223 K (950 °C) for 17 h, then at 773 K (500 °C) for 4 h and finally the furnace was cooled down to RT. X-ray diffraction showed that the composites were orthorhombic over the whole concentration range ($0 \leqslant x \leqslant 0.3$). The critical temperature, T_c, estimated from magnetic susceptibility and resistivity measurements, was $T_c = 92$ K for $x = 0$ and $T_c = 93.5$ K for the composite samples. The presence of gold in the composite has no influence on the oxygen concentration determined by chemical titration. The samples used in XPS investigations have the shape of slices with a diameter of 15 mm and approximately 1 mm thick.

The XPS spectra were measured with a VG Escalab Mk II spectrometer using non-monochromatized AlK_α ($h\nu = 1486.6$ eV) at a base pressure of 5×10^{-8} Pa. The spectrometer was calibrated using $Au(4f_{7/2})$ and $Cu(2p_{3/2})$ photoelectron lines at a binding energy (BE) of 83.8 ± 0.1 eV and 932.7 ± 0.1 eV, respectively [8]. The data were evaluated using a DEC Micro/PDP-11 computer and VG scientific model VGS 500 data processing software. All the spectra were recorded at room temperature.

It is well known that the HTSC reacts with air to form insulating surface species and it is necessary to clean the surface in an ultrahigh vacuum (UHV) system. The sample surface was prepared by three different procedures as follows. The sample was mechanically polished using abrasive paper (no. 1000) in air just before introducing to the measuring chamber (procedure A). Then the sample was carefully heated to 723–773 K (450–500 °C) in UHV for a short time, i.e. 2–3 min (procedure B). Alternatively, the sample was chemically etched for 30 s in 10% HCl in absolute methanol [9, 10] followed by short annealing in UHV under the same heating conditions (procedure C).

3. Results and discussion

3.1. Wide-range spectrum

Typical wide energy scans of the $YBa_2Cu_3O_7$ and $YBa_2Cu_3O_7$–Au composite samples obtained in the above experimental conditions are shown in Figs 2 and 3 on a binding energy (BE) scale. No charging effects in the spectra were observed. Identification of the photoelectron lines was performed as given elsewhere [3]. The spectra were recorded for the samples prepared by procedure C, i.e. after chemical etching

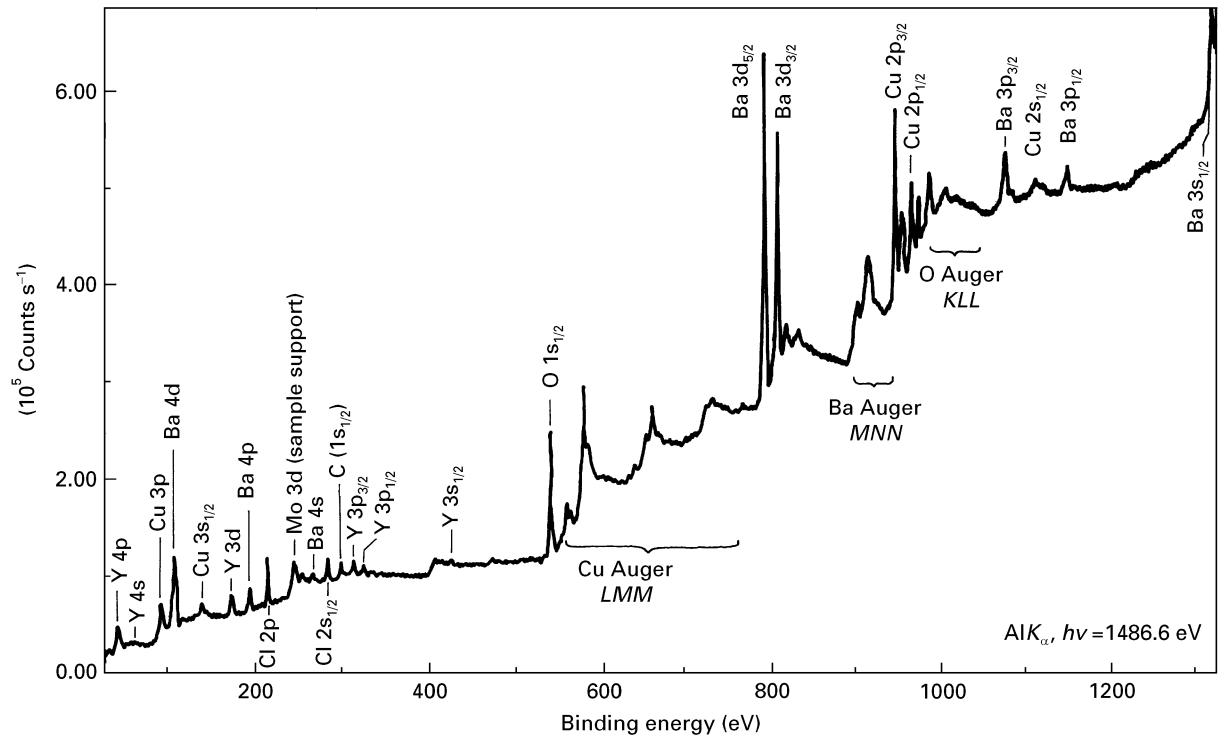

Figure 2 0–1300 eV photoemission intensity distribution of the $YBa_2Cu_3O_7$ sample. The spectrum exhibits the strongest core lines of the individual components: Y(3d), O(1s), Ba(3d), Cu(2p) and contaminations: Cl(2p) and C(1s). The X-ray excited Cu (*L M M*), Ba(*M N N*) and O(*K L L*) Auger transitions also appear clearly in the spectrum.

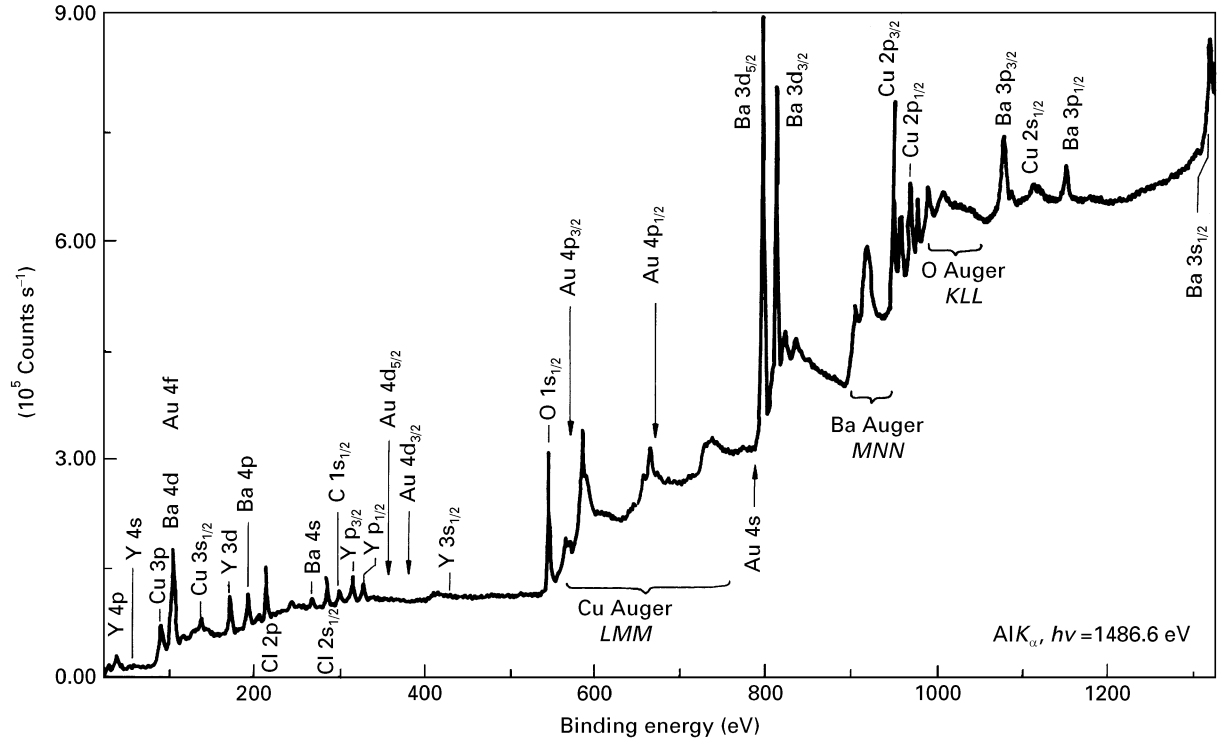

Figure 3 0–1300 eV photoemission intensity distribution of a $YBa_2Cu_3O_7$–Au composite. The spectrum exhibits the strongest core lines of the individual components: Au(4f), Y(3d), O(1s), Ba(3d), Cu(2p) and contaminations: Cl(2p) and C(1s). The X-ray excited Cu (*L M M*), Ba(*M N N*) and O(*K L L*) Auger transitions also appear clearly in the spectrum.

and preheating in UHV conditions. The $YBa_2Cu_3O_7$ spectrum, apart from the strongest core lines of the individual components, shows residual peaks coming from contaminations: C($1s_{1/2}$) at BE $\simeq$ 285 eV and Cl($2p_{3/2}$) at BE $\simeq$ 199 eV, Cl($2s_{1/2}$) at BE $\simeq$ 269 eV (Fig. 2). The C and Cl Auger peaks are invisible, indicating a very low level of contaminants on the surface. Oxygen atoms are represented by the O($1s_{1/2}$) peak at BE $\simeq$ 531 eV and the O(*K L L*) Auger series of peaks lying in the range of 970–1015 eV. Copper contributes to the photoelectron spectrum through the following features: Cu(3p) at BE $\simeq$ 74 eV, Cu(3s)

at BE $\simeq$ 123 eV, Cu($2p_{1/2}$) and Cu($2p_{3/2}$) from the range 930–960 eV and Cu($2s_{1/2}$) at BE $\simeq$ 1097 eV. X-ray induced Auger Cu(*L M M*) transitions cover the region of 540–720 eV on a BE scale. The yttrium lines Y(4p) at BE $\simeq$ 25 eV, Y(3d) at BE $\simeq$ 160 eV and Y(3p) at BE $\simeq$ 310 eV, appear in the spectrum. The Y(4s) and Y(3s) peaks are of very low intensity in Fig. 2. Finally, the barium photoelectron peaks appears in the order: Ba(4d) at BE $\simeq$ 90 eV, Ba($4p_{3/2}$) at BE $\simeq$ 178 eV, Ba(4s) at BE $\simeq$ 254 eV, the strongest lines of the spectrum Ba(3d) at 770–800 eV region, Ba($3p_{3/2}$) at BE $\simeq$ 1063 eV, Ba($3p_{1/2}$) at BE $\simeq$ 1135 eV and Ba($3s_{1/2}$) at BE $\simeq$ 1298 eV. The Ba($4p_{1/2}$) of small intensity overlap with Cl($2p_{3/2}$) line in the wide-range XPS spectrum. The peaks in Fig. 3 correspond to the identified lines from Fig. 2. The strongest Au(4f) line overlaps with the Ba(4d) peak, and because of relative small quantity of gold in the sample, the Au(4d) peaks are invisible in wide-range XPS spectrum.

3.2. Analysis of the O(1s) line shape

The O($1s_{1/2}$) peak was analysed from the point of view of cleanliness of the sample surface. Fig. 4 shows the O($1s_{1/2}$) peak registered after different procedures of sample surface preparation. The results of curve fitting are collected in Table I. The O($1s_{1/2}$) spectrum consists of two components: low and high binding-energy peaks were both observed on the samples after each cleaning procedure. The low BE peak shifts towards higher BE starting from the sample as-received (BE = 528.6 eV) up to the sample after chemical etching (BE = 529.3 eV). This peak is due to O^{2-} in the bulk superconductor. The high BE peak (BE $\simeq$ 531.2 eV), corresponding partly to surface contamination, is almost totally reduced from the spectrum after chemical etching.

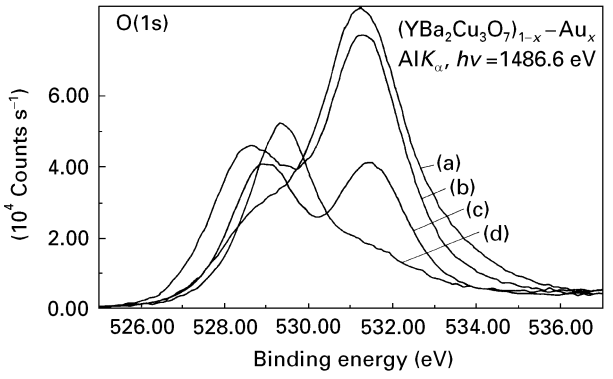

Figure 4 X-ray photoelectron spectra of the O(1s) level measured from the $YBa_2Cu_3O_7$–Au composite high-temperature superconductor sample with the preparation of the sample surface as follows: (a) as-received, (b) after mechanical polishing with abrasive paper in air, (c) after (b) followed by heating in an ultrahigh vacuum, and (d) after chemical etching and heating in an ultrahigh vacuum. For detail, see text.

Inspection of the O($1s_{1/2}$) spectra, together with the wide-range spectrum, showed that the procedure C of surface cleaning gives the best results for obtaining the bulk representative data. The high BE oxygen peak is still present in the spectrum (as a shoulder) but with reduced intensity compared to those after procedures A and B. Further results in this paper, corresponding to the true bulk of the investigated sample, come from surfaces after procedure C of cleaning.

3.3. Analysis of the Y(3d) line shape

The double Y(3d) peak obtained on both clean samples was observed at BE = 156.5 eV and BE = 157.8 eV for Y($3d_{5/2}$) and Y($3d_{3/2}$), respectively. Peak positions are in good agreement with the literature data [11] without noticeable chemical shifts. The presence of gold atoms in the $YBa_2Cu_3O_7$–Au composite sample does not perturb the environment of yttrium atoms in the lattice.

3.4. Analysis of the Ba(3d) and Ba(4d) lines

The most pronounced barium line in the XPS originates from the Ba($3d_{5/2}$) core level. In the present investigations, this line is represented as a single peak, centred at BE = 778.0 eV, with a tail on the high BE side. In both samples, the Ba(4d) photoemission peak shows easily visible double structure with maxima at BE = 87.0 eV and BE = 89.8 eV corresponding to the Ba($4d_{5/2}$) and Ba($4d_{3/2}$) core level, respectively. As above, the data are in agreement with those reported [11].

TABLE I Measured binding energy position (eV) of the O(1s) photoelectron peak for samples after different surface preparation procedures

Sample	Preparation	O(1s)	
		Low binding energy peak (eV)	High binding energy peak (eV)
$YBa_2Cu_3O_7$	As-received	528.6	531.3
	Mechanical polishing	528.6	531.1
	Chemical etching + heating	529.3	–
$YBa_2Cu_3O_7$–Au	As-received	528.6	531.2
	Mechanical polishing	528.7	531.2
	Mechanical polishing + heating	528.9	531.4
	Chemical etching + heating	529.3	–

3.5. Analysis of the Cu(2p) line shape

The most extensively investigated spectra in the past were the Cu(2p) core level spectra [12–30] of Cu, Cu_2O, CuO, $NaCuO_2$ standards and also HTSC. The Cu(2p) feature consists of two spin-orbit components: $2p_{3/2}$ and $2p_{1/2}$ separated by approximately 20 eV. In the spectrum of the Cu^{2+} compounds, apart from the main peak (M), each core level gives the satellite peak (S). Those peaks were identified to be due to $2p3d^{10}L$ final states (L indicates a ligand hole) and to $2p3d^9$ final states [12] for main and satellite peaks, respectively. Peaks for samples representing different copper valences show a shift in BE position and smaller or greater contribution of the satellite lines. The $Cu(2p_{3/2})$ spectrum of Cu_2O, i.e. of Cu^+ is characterized by one rather sharp peak at BE $\simeq$ 932.2 eV. The line of CuO, i.e. of Cu^{2+} is decidedly broader at BE $\simeq$ 933.4 eV and, as mentioned, the satellite line has 30%–50% intensity of that of the main line. The $Cu(2p_{3/2})$ of Cu^{3+} valence show a quite sharp line at BE $\simeq$ 934.8 eV without any satellite structure. Selected results concerning the Cu(2p) line which were published in the literature are collected in Table II.

In the case of HTSC, the satellite to the main intensity ratio is used in evaluation of the percentage contribution of Cu^+ and Cu^{2+} valences in the sample. Decomposition of the $Cu(2p_{3/2})$ peak into two components served as an indication of the relative presence of Cu^{2+} and Cu^{3+} valences (e.g. [21]). The fact that a contaminated surface of HTSC could give a wide range of intensity ratios and a wide range of parameters of the fitted curves, seriously complicates the consideration. For copper oxides, which can be treated as the standards for HTSC, the same behaviour was published for different treated samples before taking XPS spectra [23]. Reasonable evaluation of the different valence contributions should be based on the conviction that the $Cu(2p_{3/2})$ line broadening is due to superposition of chemically shifted lines coming from two (or three) crystallographically distinct copper sites. Such broadening should be an intrinsic property and not due to the surface contamination.

Results of the curve-fitting procedure (Fig. 5) are collected in Table III. In the first approximation, the main peak is fitted by a single, broad line. The satellite peak of near rectangular shape was decomposed into two lines. However, the $Cu(2p_{3/2})$ main line was asymmetrical in the high BE side and a second component was required for a satisfactory fit of the spectrum. Fitting was done for fixed distance in BE (equal to 1.6 eV) between two peaks of mixed Gaussian-Lorenzian line shape. The intensity of the high BE component was derived as 16% and 17%

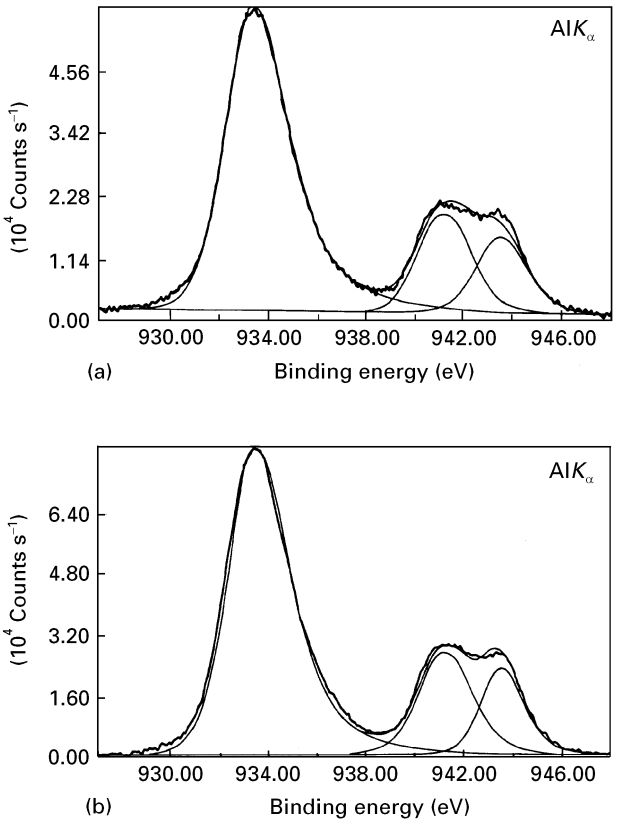

Figure 5 Experimental X-ray photoelectron spectra with rough decomposition into the one $Cu(2p_{3/2})$ peak and two satellite lines of the (a) $YBa_2Cu_3O_7$ and (b) $YBa_2Cu_3O_7$–Au composite samples.

TABLE II Reported results on $Cu(2p_{3/2})$ core level spectra. BE, binding energy; FWHM, full width at half maximum. Samples: (1) $YBa_2Cu_3O_{7-\delta}$, decomposed into three peaks [24]; (2) $La_{2-x}Sr_xCuO_4$, decomposed into three peaks [25]; (3) (Y, Sc, Ba)–Cu–O, decomposed into three peaks [27]; (4) Cu metal–Cu, Cu_2O–Cu^+, CuO–Cu^{2+}, $NaCuO_2$–Cu^{3+} [14]; (5) Cu_2O–Cu^+, CuO–Cu^{2+} [28]; (6) $Ba_{0.2}La_{1.8}CuO_{4-\delta}$–$Cu^{2+}$ [29]; (7) $Ba_2SmCu_3O_{9-\delta}$, $Ba_2YCu_3O_{9-\delta}$, decomposed into two peaks Cu^{2+}, Cu^{3+} [29]; (8) $YBa_2Cu_3O_{7-\delta}$, decomposed into two peaks Cu^{2+}, Cu^{3+} [17]

Sample	Cu		Cu^+		Cu^{2+}		Cu^{3+}	
	BE (eV)	FWHM (eV)	BE (eV)	FWHM (eV)	BE (eV)	FWHM (eV)	BE (eV)	FWHM (eV)
1.	–	–	931.5	1.56	932.6	1.56	934.2	1.56
2.	–	–	933.0	–	934.3	–	935.7	–
3.	–	–	931.9	1.56	933.0	1.56	934.6	1.56
4.	932.8	1.10	932.7	1.40	933.6	3.20	934.9	1.60
5.	932.7	1.17	932.5	1.39	933.6	1.30	–	–
6.	–	–	–	–	933.2	1.57	–	–
7.	–	–	–	–	932.8	1.57	934.8	1.57
8.	–	–	–	–	932.8	1.46	934.9	1.46

of the total $Cu(2p_{3/2})$ intensity for $YBa_2Cu_3O_7$ and $YBa_2Cu_3O_7$–Au composite, respectively. These percentages correspond roughly to the Cu^{3+} valence contribution. The results of the fits are given in Table IV.

After thorough synthesis of the $Cu(L_3M_{45}M_{45})$ Auger transition for both samples, the $Cu(L_3M_{45}M_{45})$–$Cu(2p_{3/2})$ Auger parameter was determined to belong to the range 1847.2–1847.4 eV. The values fall in line with those of CuO and Cu_2O Auger parameter boxes.

3.6. Analysis of the Au(4f) and Au(4d) line shape

The valence state of gold in the composite sample is determined from the chemical shift of the binding energy of the Au(4f) and the Au(4d) line. Published data on different gold valence states [31] and the spectra obtained in the experiments with the gold metal and $NaAuCl_4$ (Au^{3+}) were used as the reference spectra. In the $YBa_2Cu_3O_7$–Au composite, the Au(4f) core level lines partly overlap more strongly in this case with the Ba(4d) doublet. The presence of gold in the sample is manifested as a shoulder of the Ba(4d) in the BE range 84–85 eV. Decomposition of the spectrum of the 70–100 eV BE region, gives the parameters of the $Au(4f_{7/2})$ peak. The $Au(4f_{5/2})$ line could not be extracted from the spectra. The determined BE position of the $Au(4f_{7/2})$ peak and other published data are collected in Table V. The curve-fitting procedure for the Au(4d) doublet is much more straightforward. Both peaks, clearly visible in the spectrum, are found at BE = 336.3 and 354.5 eV for $Au(4d_{5/2})$ and $Au(4d_{3/2})$, respectively.

On the basis of the collected BE positions (Table V), the presence of gold in the Au^{3+} valence state could be ruled out. It was shown using XPS [32] and diffraction of electrons, X-rays and neutrons [5, 33], that gold cations, as in the case of Au_2O_3, are in the 3 + state. From results presented here, more probable for gold is the 1 + and/or 2 + oxidation state. Despite the mentioned difficulties during peak synthesis introducing error in the determination of the peak position and disagreement with those reported, it seems to be a reasonable conclusion.

3.7. Analysis of the valence band spectra

The XPS valence band (VB) spectrum of the $YBa_2Cu_3O_{7-\delta}$ compound shows a broad peak

TABLE III Curve fit to the $Cu(2p_{3/2})$ main (M) and satellite (S_1, S_2) lines of the $YBa_2Cu_3O_7$ and $YBa_2Cu_3O_7$–Au composite samples. $\Delta(S_1 - M)$ (eV), energy difference between first satellite and main peak; $I(S)/I(M)$, intensity ratio of both satellites to main peak

Sample	Main		Satellites		$\Delta(S_1 - M)$	$I(S)/I(M)$
	BE (eV)	FWHM (eV)	BE (eV)	FWHM (eV)		
$YBa_2Cu_3O_7$	933.2	2.60	941.0 943.4	2.40 2.40	7.8	0.47
$YBa_2Cu_3O_7$–Au	933.4	2.60	941.1 943.5	2.40 2.00	7.7	0.48

TABLE IV Decomposition of the $Cu(2p_{3/2})$ main line into two components for $YBa_2Cu_3O_7$ and $YBa_2Cu_3O_7$–Au composite samples. The BE distance between two components was fixed to equal 1.6 eV in the spectra

Sample	Cu^{2+}		Cu^{3+}		$I(Cu^{3+})$
	BE (eV)	FWHM (eV)	BE (eV)	FWHM (eV)	$[I(Cu^{2+}) + I(Cu^{3+})]$
$YBa_2Cu_3O_7$	933.3	3.00	934.9	2.57	16%
$YBa_2Cu_3O_7$–Au	933.4	3.00	935.0	2.64	17%

TABLE V Binding energy position of the Au(4f) and the Au(4d) photoelectron peaks of the gold reference, $NaAuCl_4$ and $YBa_2Cu_3O_7$–Au composite samples

Sample	Binding energy (eV)			
	$Au(4f_{7/2})$	$Au(4f_{5/2})$	$Au(4d_{5/2})$	$Au(4d_{3/2})$
Au metal (Au 0)	83.7	87.4	335.1	353.4
Au^+	84.4			
Au^{2+}	86.3			
$NaAuCl_4$ (Au^{3+}) [31]	87.5	90.9	337.2	355.5
$(YBa_2Cu_3O_7)_{1-x}$–Au_x $x \leqslant 0.3$	84.0			
This work	84.2		336.3	354.5

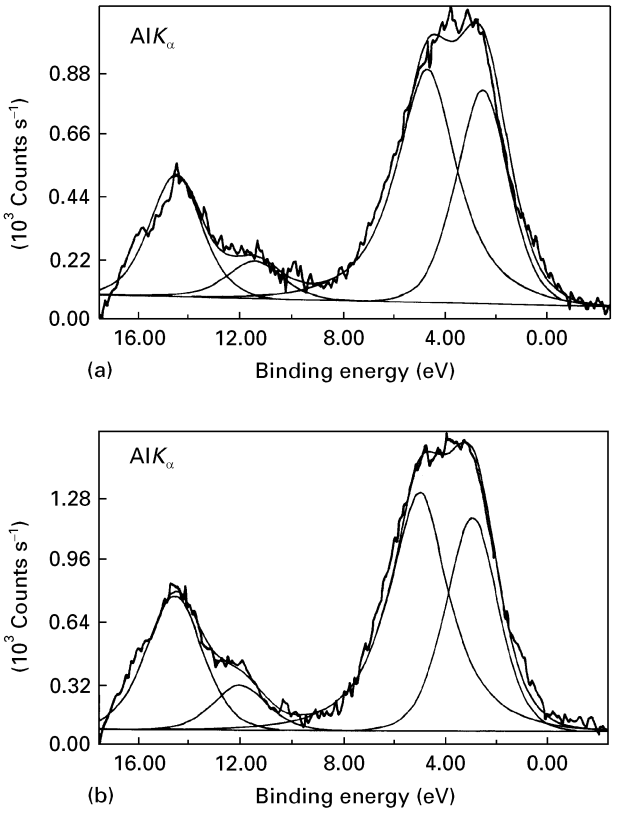

Figure 6 X-ray photoelectron spectra of the valence band region in (a) $YBa_2Cu_3O_7$ and (b)$YBa_2Cu_3O_7$–Au composite. Three prominent structures, A, C and D, are observed and band A exhibits a doublet structure.

(FWHM $\simeq$ 4 eV) centred at around 4 eV below the Fermi level, E_F. The peak could be decomposed into two features: at BE $\simeq$ 2.5 and BE $\simeq$ 4.5 eV, which are associated with the Cu(3d) band but in some papers the second peak is assigned as the O(2p) level (e.g. [34]). The contribution of the Y($4d_{5/2}$) (BE $\simeq$ 3 eV) to the density of states of the valence band is negligible [3]. In contrast, some authors claim that a small shoulder observed approximately at 1 eV below E_F, should be attributed to the O(2p) state, which tends to be located near the Fermi level [35]. The valence band spectra also exhibit features at BE $\simeq$ 9.5 and 12.5 eV. The chemical origin of the first one is unclear and it is assigned to the C(2s) state, because of carbon which is coming from the starting materials for preparation of the compound. The second structure was assigned to the Ba(5p) state and/or to the valence band satellite, as was observed in copper and its compounds such as oxides [35].

The VB region of the $YBa_2Cu_3O_7$ sample and $YBa_2Cu_3O_7$–Au composite are presented in Fig. 6. As expected, the density of states at E_f, negligible for the green-phase ceramic [3], is relatively large for pure $YBa_2Cu_3O_7$ and its gold composite, showing their metallic character. To be consistent with Godowski *et al.* [3], the spectra are decomposed into three regions: the broad peak closest to the E_F as A_1 and A_2 constituents and the two remaining peaks as C and D features. The peak near the Fermi level is wider in the case of the $Y_2Cu_2O_5$–Au and the intensity ratio of A_1/A_2 indicates a greater contribution of A_2 to the band (Table VI). The relative intensity of peak C was observed in the range 0.17–0.21. Peak D, corresponding to the Ba(5p) level, appears at BE = 14.6 and 14.7 eV for the $YBa_2Cu_3O_7$ and $YBa_2Cu_3O_7$–Au composite samples, respectively.

TABLE VI Summary of the X-ray photoelectron valence band spectra of the $(YBa_2Cu_3O_7)_{1-x}$–Au_x samples. Bands A, C and D are recognized (see text) as A_1–Cu(3d), A_2–Cu(3d) with or without the contribution of O(2p); C, valence band satellite; D, Ba(5p)

Sample	Binding energy (eV)				Intensity ratio	
	A_1	A_2	C	D	A_1/A_2	C/A_1
$YBa_2Cu_3O_7$	2.60	4.80	11.5	14.6	0.73	0.17
$YBa_2Cu_3O_7$–Au	3.00	5.10	12.1	14.7	0.71	0.21

The presence of incorporated gold atoms shows little influence on the VB spectra, almost negligible in comparison with the core-level spectra. The VB spectra are similar to the green phase ceramic spectra [3] and to those reported in the literature for fully oxygenated $YBa_2Cu_3O_7$ [10, 36, 37].

4. Conclusions

The results of the present XPS study of $(YBa_2Cu_3O_4)_{1-x}$–Au_x composite samples are summarized as follows.

1. Chemical etching of the samples was confirmed as the best procedure method for sample surface cleaning.
2. The incorporated gold atoms in the material are in the valence state which lies between 1 + and 2 + .
3. The presence of gold does not introduce any change in the valence states of the remaining components, i.e. of yttrium, barium, copper and oxygen.

Acknowledgements

The authors thank Dr Philippe Marcus, Director of the Laboratory, for permission to perform XPS measurements and for his help during investigations.

References

1. C. R. BRUNDLE and D. E. FOWLER, *Surf. Sci. Rep.* **19** (1993) 143.
2. P. A. P. LINDBERG, Z.-X. SHEN, W. E. SPICER and I. LINDAU, *ibid.* **11** (1990) 1.
3. P. J. GODOWSKI, C. HINNEN, R. HORYN and J. KLAMUT, in preparation.
4. H. OYANAGI, H. IHARA, T. MATSUBARA, M. TOKUMOTO, T. MATSUSHITA, M. HIRABAYASHI, K. MURATA, N. TERADA, T. YAO, H. IWASAKI and Y. KIMURA, *Jpn J. Appl. Phys.* **26** (1987) L1561.
5. M. Z. CIEPLAK, G. XIAO, C. L. CHIEN, A. BAKHSHAI, D. AKTYMOWICZ, W. BYDEN, J.K. STALICK and J. J. RHYNE, *Phys. Rev. B* **42** (1990) 6200.
6. M. Z. CIEPLAK, G. XIAO, C. L. CHIEN, J. K. STALICK and J. J. RHYNE, *Appl. Phys. Lett.* **57** (1990) 934.
7. C. NGUYEN VAN HUONG, M. NICOLAS, A. DUBON and C. HINNEN, *J. Mater. Sci.* **28** (1993) 6418.
8. D. FUJITA and K. YOSHIHARA, *Surf. Interface Anal.* **21** (1994) 226.

9. R. P. VASQUEZ and W. L. OLSON, *Phys. C* **177** (1991) 223.
10. R. P. VASQUEZ, M. C. FOOTE, L. BAJUK and B. D. HUNT, *J. Electron. Spectrosc. Rel. Phenom.* **57** (1991) 317.
11. D. E. FOWLER, C. R. BRUNDLE, J. LERCZAK and F. HOLTZBERG, *ibid.* **52** (1990) 323.
12. A. BIANCONI, A. CONGIU-CASTELLANO, M. De SANTIS, P. DELOGU, A. GARGANO and R. GIORGI, *Solid State Commun.* **63** (1987) 1135.
13. N. FUKUSHIMA, H. YOSHINO, H. NIU, M. HAYASHI, H. SASAKI, Y. YAMADA and S. MURASE, *Jpn J. Appl. Phys.* **26** (1987) L 719.
14. P. STEINER, V. KINSINGER, I. SANDER, B. SIEGWART, S. HUFNER, C. POLITIS, R. HOPPE and H. P. MULLER, *Z. Phys. B Cond Matter* **67** (1987) 497.
15. T. A. SASAKI, Y. BABA, N. MASAKI and I. TAKANO, *Jpn J. Appl. Phys.* **26** (1987) L 1569.
16. F. WERFEL, M. HEINONEN and E. SUONINEN, *Z. Phys. B Cond. Matter.* **70** (1988) 317.
17. T. GOURIEUX, G. KRILL, M. MAURER, M. F. RAVET, A. MENNY, H. TOLENTINO and A. FONTAINE, *Phys. Rev. B* **37** (1988) 7516.
18. P. STEINER, S. HUFNER, V. KINSINGER, I. SANDER, B. SIEGWART, H. SCHMITT, R. SCHULZ, S. JUNK, G. SCHWITZGEBEL, A. GOLD, C. POLITIS, H. P. MULLER, R. HOPPE, S. KEMMLKER-SACK and C. KUNZ, *Z. Phys. B Cond. Matter.* **69** (1988) 449.
19. A. BALZAROTTI, M. De CRESCENZI, N. MOTTA, F. PATELLA and A. SGARLATA, *Phys. Rev. B* **38** (1988) 6461.
20. J. M. MARIOT, V. BARNOLE, C. F. HAGUE, G. VETTER and F. QUEYROUX, *Z. Phys. B Cond. Matter.* **75** (1989) 1.
21. P. ADLER, H. BUCHKREMER-HERMANNS and A. SIMON, *ibid.* **84** (1990) 1.
22. F. PARMIGIANI, L. E. DEPERO, T. MINERVA and J. B. TORRANCE, *J. Electron Spectrosc. Rel. Phenom.* **58** (1992) 315.
23. R. V. SIRIWARDANE and J. A. POSTON, *Appl. Surf. Sci.* **68** (1993) 65.
24. H. IHARA, M. HIRABAYASHI, N. TERADA, Y. KIMURA, K. SENZAKI, M. AKIMOTO, K. BUSHIDA, F. KAWASHIMA and R. UZUKA, *Jpn J. Appl. Phys.* **26** (1987) L460.
25. H. IHARA, M. HIRABAYASHI, N. TERADA, Y. KIMURA, K. SENZAKI and M. TOKUMOTO, *ibid.* **26** (1987) L 463.
26. P. J. GODOWSKI and P. MARCUS, *Acta Phys. Polon.* **A 87** (1995) 619.
27. N. MORI, Y. TAKANO and H. OZAKI, *Jpn J. Appl. Phys.* **26** (1987) 1017.
28. G. DEROUBAIX and P. MARCUS, *Surf. Interface Anal.* **18** (1991) 39.
29. F. GARCIA-ALVARADO, E. MORAN, M. VALLET, J. M. GONZALEZ-CALBET, M. A. ALARIO, M. T. PEREZ-FRIAS, J. L. VINCENT, S. FERRER, E. GARCIA-MICHEL and M. C. ASENSIO, *Solid State Commun.* **63** (1987) 507.
30. P. J. GODOWSKI and E. L. HARDEGREE, *Acta Phys. Polon.* **A 85** (1994) 843.
31. K. KISHI and S. IKEDA, *J. Phys. Chem.* **78** (1974) 107.
32. A. F. HAPP, J. R. GAIER, J. J. POUCH and P. D. HAMBURGER, *J. Solid State Chem.* **74** (1988) 433.
33. H. RENEVIER, J. L. HODEAU, T. FORANIER, P. BARDET and M. MAREZIB, *Phys. C* **172** (1990) 183.
34. A. J. ARKO, R. S. LIST, R. J. BARTLETT, S. W. CHEONG, Z. FISK, J. D. THOMPSON, C. G. OLSON, A. B. YANG, R. LIU, C. GU, B. W. VEAL, J. Z. LIU, A. P. PAULIKAS, K. VANDERVOORT, H. CLAUS, J. C. CAMPUZANO, J. E. SCHIRBER and N. D. SHINN, *Phys. Rev. B* **40** (1989) 2268.
35. T. TAKAHASHI, F. MAEDA, H. ARAI, H. KATAYAMA-YOSHIDA, Y. OKABE, T. SUZUKI, S. HOSOYA, A. FUJIMORI, T. SHIDARA, T. KOIDE, T. MIYAMARA, M. ONODA, S. SHAMOTO and M. SATO, *ibid.* **36** (1987) 5686.
36. A. FUJIMORI, E. TAKAYAMA-MUROMACHI, Y. UCHIDA and B. OKAI, *ibid.* **35** (1987) 8814.
37. M. H. FROMMER, *ibid.* **38** (1988) 2444.

Received 10 April 1995
and accepted 13 June 1996